

Facile Synthesis of Sulfur-Containing Transition Metal (Mn, Fe, Co, and Ni) (Hydr)oxides for Efficient Oxygen Evolution Reaction

Feng Zeng,^[a] Cornelia Broicher,^[a] Jan P. Hofmann,^[b] Stefan Palkovits,^[a] and Regina Palkovits^{*[a]}

Transition metal based materials are promising non-noble metal based catalysts for the oxygen evolution reaction (OER). Transition metal (hydr)oxides have been intensively investigated as OER catalysts. Promoting transition metal (hydr)oxides with heteroatoms or using carbon materials as additives can increase the electric conductivity and tailor the nature of active sites to enhance OER activity. We developed a scalable one-step wet chemical method to prepare sulfur-containing transition metal (manganese, iron, cobalt, and nickel) (hydr)oxides coupled with carbon nanotubes as additives to tailor OER performance. Facilitated OER kinetics, enhanced intrinsic activity, and high electrochemically active surface area derived from sulfur promotion with/without carbon nanotubes addition together with the nanostructure of the materials led to decent OER performance. Sulfur-containing cobalt (hydr)oxide achieved a low overpotential of 0.38 V at 10 mA cm⁻², a low Tafel slope of 66 mV dec⁻¹, and good stability.


Electrochemical water splitting is a promising technology to produce hydrogen (H₂) as a green energy carrier.^[1–3] However, a practical application of the technology is hampered by the sluggish kinetics (high overpotential) of the anodic oxygen evolution reaction (OER).^[4,5] Various catalysts have been investigated to accelerate the kinetics and reduce the overpotential of OER,^[3–6] and iridium/ruthenium based materials are among the most active catalysts for OER in acid conditions and also possess relatively high activity in basic conditions.^[7–10] However, the scarcity and the high cost of iridium/ruthenium impede their


large-scale utilization in industry. Transition metal based materials have been intensively investigated to substitute iridium/ruthenium based materials due to their high abundance in the earth's crust and their lower costs.^[11–13] Diverse strategies have been developed to improve the OER performance of transition metal based materials.^[13,14] Such strategies include, 1) creating nanostructures and reducing the catalyst size to raise the exposure of active sites and the electrochemically active surface area;^[15,16] 2) increasing the electric conductivity by coupling the catalyst with conductive compounds like nickel foam,^[17] transition metal chalcogenides,^[18] and carbon materials;^[19] 3) tailoring the intermediate adsorption and the intrinsic activity by elemental doping,^[20,21] defect engineering,^[22] and coating with carbon materials.^[23] Recent studies showed that transition metal based materials, MX_aY_b (M = transition metal, X, Y = O, S, Se, N, and P), possess good OER performance.^[24–28] The incorporation of a second element can optimize the electronic structure, create active sites, and facilitate the intermediate adsorption to achieve high electric conductivity, high exposure of active sites, and high intrinsic activity for decent electrochemical oxygen evolution performance.^[24–28] However, MX_aY_b type materials are usually prepared by multi-step methods, including high-temperature sulfurization, selenization, phosphorization, nitridation, or N₂ plasma treatment.^[25–28] Thus, it is important to develop facile one-step wet chemical methods to provide an efficient access to MX_aY_b type materials for OER.

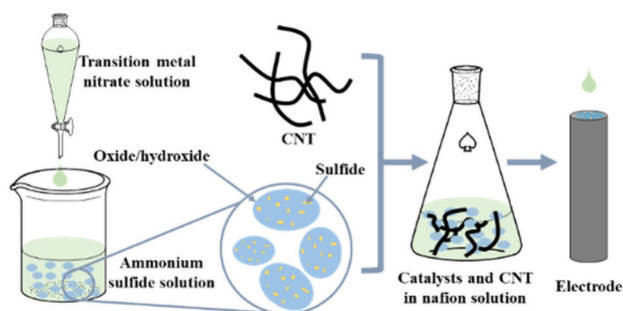
Herein, we report a facile one-step wet chemical method to prepare sulfur-containing transition metal (hydr)oxides by precipitation of transition metal nitrate solutions with an ammonium sulfide solution to result in efficient OER catalysts. Nanostructured sulfur-containing manganese, iron, cobalt, and nickel (hydr)oxide were obtained. Carbon nanotubes (CNT) used to tailor the OER performance were added into the catalyst ink when preparing the electrode. The incorporation of sulfur and carbon nanotubes together with the materials' nanostructure led to enhanced electric conductivity, tailored active sites, improved intrinsic activity, and high exposure of the active sites resulting in decent OER activity. The optimized sulfur-containing cobalt (hydr)oxide achieved a low overpotential of 0.38 V at a current density of 10 mA cm⁻², a low Tafel slope of 66 mV dec⁻¹, and a good stability. The benchmarking NiFeO_x was synthesized for comparison,^[29] the overpotential of CoOS is comparable to 0.36 V of NiFeO_x. The facile method for synthesizing sulfur-containing transition metal (hydr)oxides can be extended to other transition metals and bimetal based materials for efficient OER catalysts.

[a] F. Zeng, C. Broicher, S. Palkovits, Prof. R. Palkovits
Chair of Heterogeneous Catalysis and Chemical Technology
Institut für Technische und Makromolekulare Chemie
RWTH Aachen University
Aachen 52074 (Germany)
E-mail: palkovits@itmc.rwth-aachen.de

[b] Dr. J. P. Hofmann
Laboratory for Inorganic Materials and Catalysis
Department of Chemical Engineering and Chemistry
Eindhoven University of Technology
Eindhoven 5600 MB (The Netherlands)

 Supporting information for this article is available on the WWW under <https://doi.org/10.1002/cctc.201901493>

 © 2019 The Authors. Published by Wiley-VCH Verlag GmbH & Co. KGaA. This is an open access article under the terms of the Creative Commons Attribution Non-Commercial License, which permits use, distribution and reproduction in any medium, provided the original work is properly cited and is not used for commercial purposes.



Scheme 1. Preparation of sulfur-containing transition metal (hydr)oxides and the corresponding electrodes.

The sulfur-containing transition metal (hydr)oxides were prepared by precipitation of transition metal nitrate solution with ammonium sulfide solution at room temperature. The preparation of the materials and electrode is presented in Scheme 1. The transition metal nitrate solution was added dropwise to the ammonium sulfide solution. The (hydr)oxides were formed due to the ololation/oxolation of the transition metal ions. The reaction of S^{2-} with transition metal ions or transition metal (hydr)oxide led to the formation of sulfur-containing species. CNT can be incorporated easily by mixing in the Nafion solution followed by ultra-sonication. With this method, we simplified the complex multistep synthesis of MO_xS_b into a facile one-step method overcoming the need for high temperature sulfurization. The one-step room temperature wet chemical synthesis has potential to be scaled up for mass production. The sulfur-containing manganese, iron, cobalt, and

Table 1. Composition of the synthesized materials obtained by EDX.

	TM [at.%] ^[a]	O [at.%] ^[b]	S [at.%] ^[c]
MnOS	33.9	49.3	16.8
FeOS	31.0	47.1	21.9
CoOS	36.7	45.4	17.9
NiOS	44.9	29.6	25.5

[a] The atomic percent of transition metal, [b] The atomic percent of oxygen, [c] The atomic percent of sulfur.

nickel (hydr)oxide were designated as MnOS, FeOS, CoOS, and NiOS, respectively. The composition of the synthesized materials was analyzed by energy-dispersive X-ray spectroscopy (EDX). Figure S1 presents the EDX spectra of the obtained materials, and the atomic percent is summarized in Table 1. The existence of the corresponding transition metal, oxygen, and sulfur peaks in EDX spectra indicated the formation of transition metal-oxygen-sulfur compounds. The transition metal content reached 31.0–44.9 at.%, oxygen contributed 29.6–49.3 at.%, and the sulfur content accounted for 16.8–25.5 at.%, respectively.

Figure 1 shows the X-ray diffraction (XRD) patterns of the synthesized materials and the corresponding reference patterns. MnOS contained Mn_3O_4 as major crystalline phase. FeOS consisted of α -FeOOH and γ -FeOOH. Due to the poor crystallinity of CoOS and NiOS, it was difficult to determine the crystal phases. CoOS was possibly composed of poorly crystallized CoOOH and $Co(OH)_2$, and NiOS was comprised of poorly crystallized $Ni(OH)_2$. In general, the low signal to noise ratio of all materials indicates low crystallinity and/or a major fraction of amorphous phases, which may be the reactive species.^[30]

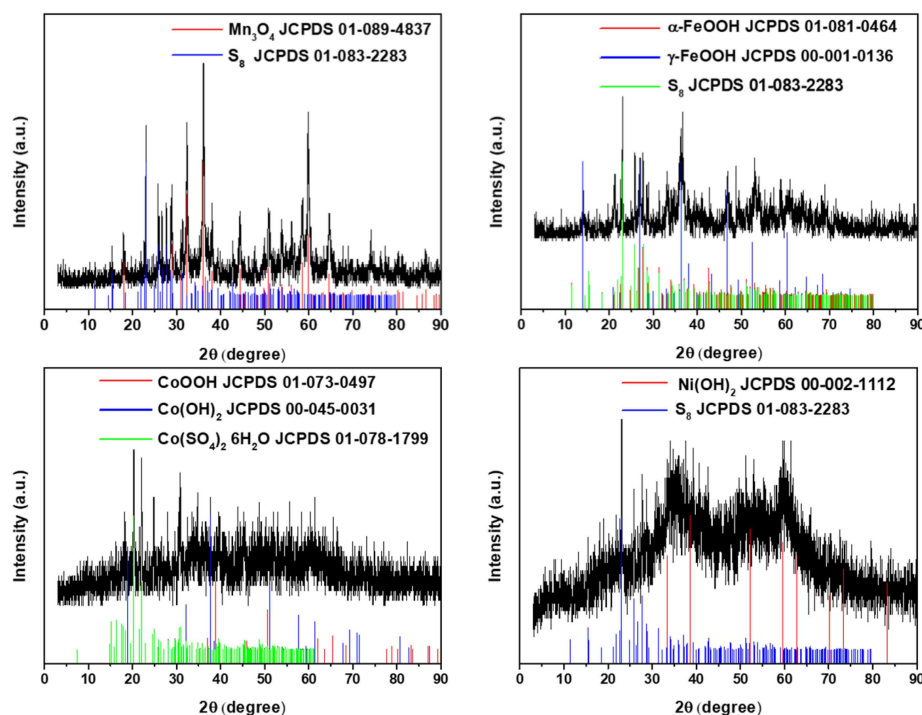


Figure 1. XRD patterns and the corresponding reference patterns of the synthesized materials, MnOS (a), FeOS (b), CoOS (c), and NiOS (d).

Transition metal sulfate and S_8 , which may be formed through the oxidation of sulfur due to air exposure were also present in the obtained materials.

Figure 2 presents the S 2p X-ray photoelectron spectra (XPS) of the obtained materials. The S 2p spectra can be deconvoluted into three doublets, $BE(S\ 2p_{3/2}) = 168.66 \pm 0.21\text{ eV}$ and $BE(S\ 2p_{1/2}) = 169.84 \pm 0.21\text{ eV}$ for SO_4^{2-} , $BE(S\ 2p_{3/2}) = 164.23 \pm 0.38\text{ eV}$ and $BE(S\ 2p_{1/2}) = 165.41 \pm 0.38\text{ eV}$ for S^0 , $BE(S\ 2p_{3/2}) = 162.41 \pm 0.47\text{ eV}$ and $BE(S\ 2p_{1/2}) = 163.59 \pm 0.47\text{ eV}$ for S^{2-} .^[31–36] While XPS confirms the presence of sulfide groups, no crystalline sulfur containing phases could be observed by XRD. This may be due to the formation of very small crystals or a surface layer, which is potentially XRD amorphous. The sulfide plays an important role for enhancing OER activity because of the high electric conductivity and a synergistic electronic interactions with (hydr) oxides.^[37] Figure 3 presents the morphologies of the sulfur-containing transition metal (hydr)oxides observed by scanning electron microscopy (SEM). MnOS, CoOS, and NiOS possessed nano-spheres, and FeOS was composed of nano-plates. These nanostructures enabled a high exposure of surface sites as supported by the relatively high electrochemically surface area compared with the benchmarking catalysts reported in the literature (Figure S2).

We investigated the sulfur-containing transition metal (hydr)oxides as potential electrocatalyst for OER. Figure 4 (a) presents the polarization curves of the sulfur-containing transition metal (hydr)oxides. MnOS and FeOS showed very low OER activity, the current densities at a potential of 1.8 V versus RHE (reversible hydrogen electrode) were less than 2 mA cm^{-2} .

CoOS and NiOS possessed good OER activities, and both catalysts reached a current density of 10 mA cm^{-2} at a potential of about 1.64 V versus RHE. To tailor the OER performance of the sulfur-containing transition metal (hydr)oxides, CNT were incorporated when preparing the catalyst ink. The materials with CNT were designated as MOS–C (M=transition metal). CNT only slightly influenced the OER activities of CoOS and NiOS. The potentials at 10 mA cm^{-2} of CoOS–C stayed almost the same, while that of NiOS–C increases to 1.66 V versus RHE. In contrast, the OER activities of MnOS–C and FeOS–C increased significantly with CNT addition. A current density of 10 mA cm^{-2} was obtained at 1.84 and 1.73 V versus RHE, respectively (Figure 4b).

The Tafel plot was obtained by plotting the overpotential versus the logarithm of current density. A low slope of the Tafel plot indicates fast increase of the current density with increasing potential and facilitated kinetics. For catalysts without carbon nanotubes, the Tafel slopes of MnOS, FeOS, CoOS, and NiOS were 247, 98, 62, 110 mV dec^{-1} (Figure 4c), respectively. The addition of CNT shifted the Tafel slope of MnOS–C, FeOS–C, CoOS–C, and NiOS–C to 134, 73, 63, and 149 mV dec^{-1} (Figure 4d), respectively. CoOS and CoOS–C possessed the lowest Tafel slopes of 62 and 63 mV dec^{-1} , respectively. The OER kinetics of MnOS and FeOS were facilitated, while that of NiOS was deteriorated by CNT addition. The change of Tafel slopes was consistent with the results of electrochemical impedance spectroscopy (EIS) (Figure S3). The charge transfer resistances (R_{ct}) were extracted from EIS results using a two time constant equivalent circuit (Figure S3c) and summarized in Table 2. The

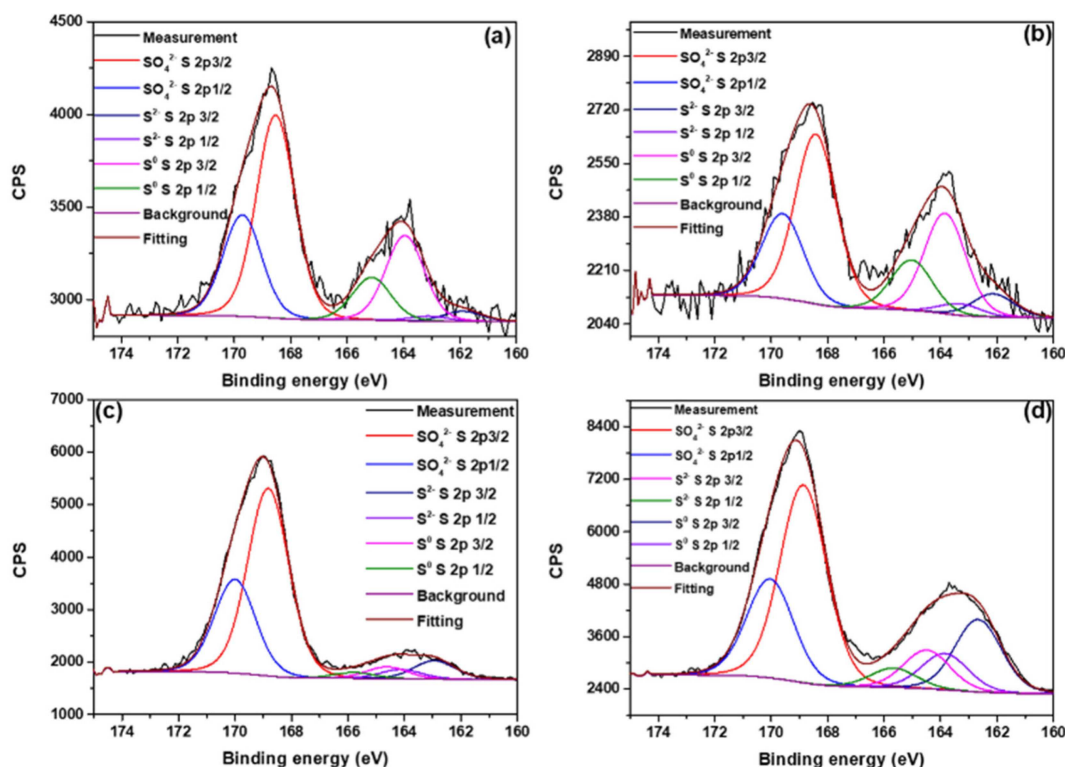


Figure 2. The S 2p XPS spectra of the synthesized materials, (a) MnOS, (b) FeOS, (c) CoOS, and (d) NiOS.

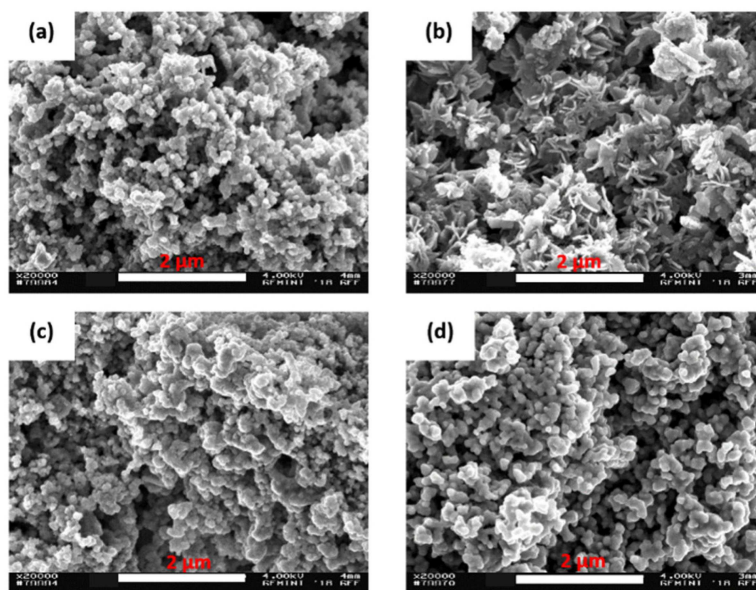


Figure 3. SEM images of the synthesized materials, MnOS (a), FeOS (b), CoOS (c), and NiOS (d). The scale bars are 2 μm .

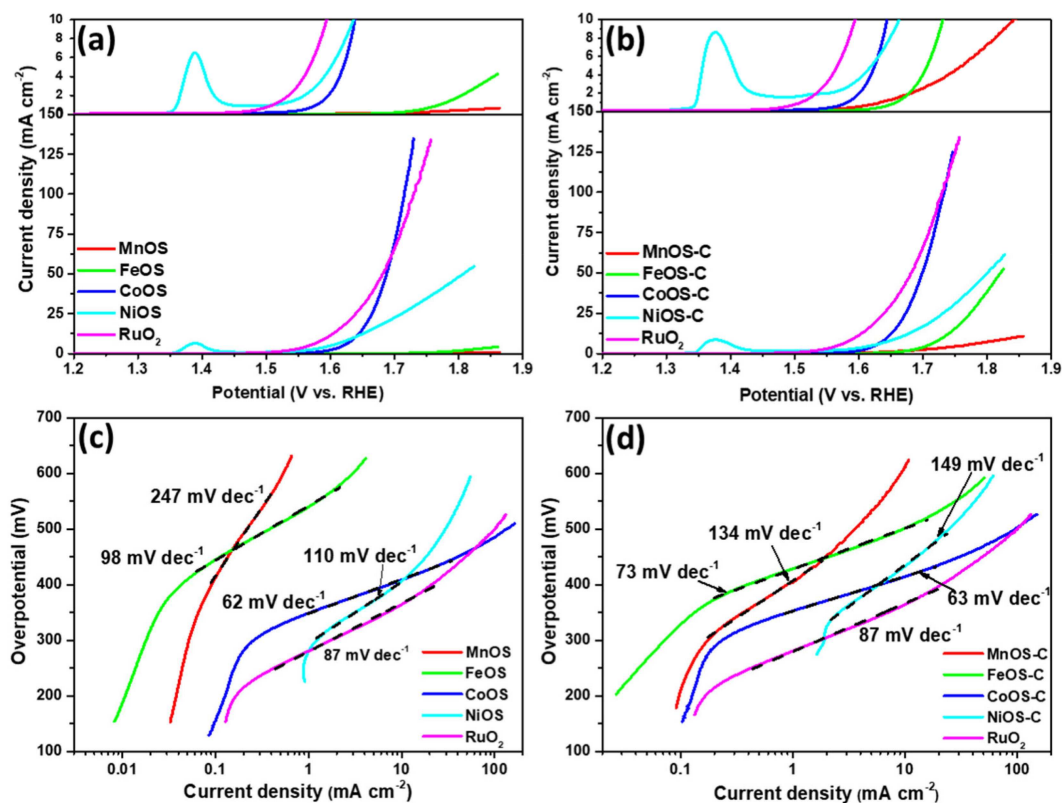


Figure 4. Electrochemical oxygen evolution performance of the sulfur-containing transition metal (hydr)oxides compared with commercial RuO_2 . Polarization curves of the sulfur-containing transition metal (hydr)oxides without (a) and with (b) CNT. Tafel plots of the sulfur-containing transition metal (hydr)oxides without (c) and with (d) CNT.

R_{ct} of MnOS and FeOS dropped significantly, while those of CoOS and NiOS increased with CNT addition. The reasons are ascribed to the change of electric conductivity and the adsorption state of the oxygenated intermediates. The electro-

chemical double layer capacitances (C_{dl}) were acquired by performing cyclic voltammetry (CV) measurement in the non-faradaic range at varying scan rate (Figure S4). With the C_{dl} results, the electrochemically active surface areas (ECSA) were

Table 2. Charge transfer resistance, electrochemical active surface area, and specific current densities.

	Without CNT $R_{ct}^{[a]}$ [Ω]	ECSA ^[b] [cm^2]	$i_s^{[c]}$ [$mA\ cm^{-2}$]	With CNT $R_{ct}^{[a]}$ [Ω]	ECSA ^[b] [cm^2]	$i_s^{[c]}$ [$mA\ cm^{-2}$]
MnOS	14341	0.39	0.052	758	4.40	0.072
FeOS	16521	0.14	0.163	1501	0.40	1.265
CoOS	57	0.69	12.613	87	0.68	9.370
NiOS	67	0.34	8.277	131	0.32	6.624
RuO ₂	43	0.91	9.068	N.A.	N.A.	N.A.
Co ₃ O ₄	161.4	0.41	8.88	N.A.	N.A.	N.A.

[a] Charge transfer resistance, [b] Electrochemically active surface area, [c] Specific current density based on electrochemically active surface area.

estimated as described in Note S1 and summarized in Table 2. The ECSA of MnOS, FeOS, CoOS, and NiOS were 0.39, 0.14, 0.69, and 0.34 cm^2 , respectively. After the incorporation of CNT, the ECSA of MnOS-C and FeOS-C increased to 4.40 and 0.40 cm^2 , respectively, while those of CoOS-C and NiOS-C only changed slightly. The reason could be that the addition of CNT increased the electric conductivity and further the availability of the active sites. However, CNT showed less influence on the electric conductivity of CoOS and NiOS and accordingly little effects on their ECSA. The influence of CNT on the ECSA of the electrode depends on the electric conductivity of the materials. CNT can increase the ECSA of poorly conductive materials significantly, while it only slightly effects more conductive materials.^[38]

To gain deeper insight into the intrinsic activity of the materials, we calculated the specific current density with the ECSA. The polarization curves based on the ECSA are presented in Figure S5, and the specific current densities at 1.7 V versus RHE are listed in Table 2. CoOS(-C) reached the highest specific current density. The overall order was MnOS(-C) < FeOS(-C) < CoOS(-C) > NiOS(-C), which is related to the adsorption strength of the oxygenated intermediates. Cobalt-based oxides possessing a moderate adsorption strength for oxygenates and located near the middle of the Volcano plot,^[39,40] showed the highest specific current density (intrinsic activity). A sulfur free nanostructured Co₃O₄ (50 nm, Aldrich) was tested for comparison. It possesses lower specific current density and higher charge transfer resistance (Table 2), indicating the positive effects of sulfur on OER activity. We also made a correlation between the charge transfer resistance normalized by ECSA (R_{ct}') and i_s (Figure S6). The specific current density decreased with increasing R_{ct}' indicating that the intrinsic activity decreased with increasing kinetic barrier.

The addition of CNT increased the specific current density of MnOS-C and FeOS-C, and decreased that of CoOS-C and NiOS-C. A potential explanation could be that the addition of CNT may shift MnOS-C and FeOS-C close to the middle of the volcano plot, while CoOS-C and NiOS-C were drawn away from the medium. The high specific current densities compared with those of the corresponding transition metal oxides reported in the literature (Figure S7) indicate that sulfur promotion with/without CNT addition by such a facile method can enhance the intrinsic OER activity. We also compared commercial RuO₂ to sulfur-containing transition metal (hydr)oxides (Figure 4). CoOS showed similar activity to RuO₂. CoOS also possessed a lower

Tafel slope of 62 $mV\ dec^{-1}$ and a higher specific current density of 12.613 $mA\ cm^{-2}$ (at 1.7 V versus RHE) compared to 87 $mV\ dec^{-1}$ and 9.068 $mA\ cm^{-2}$ of RuO₂. We further optimized the catalyst loading of CoOS, and 10 $mA\ cm^{-2}$ was achieved at an overpotential of 0.38 V with a Tafel slope of 66 $mV\ dec^{-1}$ (Figure S8), in line with the most active NiFeO_x catalyst possessing an overpotential of 0.36 V (Figure S9). CoOS showed a good stability in a chronoamperometric study with only slowly deteriorating activity within 10 hours (Figure S10). We also characterized the CoOS after long-term OER measurement. The morphology of CoOS changed from nano-spheres to nano-plates after OER test (Figure S11). Figure S12 presents the Co 2p and S 2p XPS spectra of the fresh and used CoOS. The XPS spectra indicate that CoO transformed to Co₃O₄, and the surface S⁰ and S²⁻ were oxidized after long-term OER measurement.

In summary, we report a one-step scalable wet chemical method to prepare sulfur-containing transition metal (hydr)oxides for efficient oxygen evolution reaction. By precipitation of transition metal nitrate solutions with ammonium sulfide solution, sulfur-containing transition metal (hydr)oxides were obtained through transition metal ions ololation/oxolation and sulfurization. Materials prepared by this method possessed nanostructures enabling a high exposure of active sites. The incorporation of sulfur with/without CNT addition increased the electric conductivity and tailored the nature of the active sites, leading to high intrinsic activity. With high electrochemically active surface area and enhanced intrinsic activity, sulfur-containing cobalt (hydr)oxide showed good OER performance and stability with a low overpotential of 0.38 V at 10 $mA\ cm^{-2}$ and low Tafel slope of 66 $mV\ dec^{-1}$. This versatile synthesis method can be extended to other transition metals and bimetal catalysts for efficient OER.

Experimental Section

Synthesis of sulfur-containing transition metal (hydr)oxides. Sulfur-containing transition metal (hydr)oxides, MnOS, FeOS, CoOS, and NiOS were prepared by precipitation of the corresponding transition metal nitrate (Mn(NO₃)₂·4H₂O (Carl Roth), Fe(NO₃)₃·9H₂O (Sigma-Aldrich), Co(NO₃)₂·6H₂O (Carl Roth), and Ni(NO₃)₂·6H₂O (Merck)) solution. Typically, 24 mL of the 1.2 M transition metal nitrate solution was prepared by dissolving the corresponding nitrate in deionized water. Then the transition metal solution was added into 20 mL 20 wt.% ammonium sulfide solution (Sigma-

Aldrich) drop by drop under stirring at room temperature, and the precipitate was formed. The slurry was stirred at room temperature for 10 minutes. After that, the mixture was filtered and washed with deionized water to remove the impurities. The precipitate was dried under ambient conditions for 24 hours, and sulfur-containing transition metal (hydr)oxides were obtained. Multiwall carbon nanotubes (Aldrich) used as additives for electrochemical measurements were treated with concentrated 69% nitric acid at room temperature beforehand. NiFeO_x was synthesized according to reference [29] with minor modifications for comparison. NiFeO_x was synthesized by electrodeposition in a solution containing 40 mL H_2O , 0.1 g $\text{FeSO}_4 \cdot 7\text{H}_2\text{O}$, 0.117 g $(\text{NH}_4)_2\text{SO}_4$, 0.105 g $\text{Ni}(\text{NO}_3)_2$. The pH of the solution was adjusted by H_2SO_4 to 2.5. The electrodeposition was performed at -50 mA cm^{-2} with a rotating speed of 1200 rpm for 50 s.

Characterization of the catalysts. X-ray diffraction (XRD) measurements were carried out on a Siemens D5000 diffractometer with $\text{Cu K}\alpha$ radiation ($\lambda = 0.15406 \text{ nm}$) at 45 kV and 40 mA. Scanning electron microscopy (SEM) images were taken on a ZEISS DSM 982 Gemini microscope at 4 kV. JEOL JSM-7000F scanning electron microscope coupled with a combined EDX/EBSD system (EDAX Pegasus) was used to determine the elemental composition. Five independent measurements at different sampling positions were carried out. The quantification results nearest to the average is reported in our manuscript. XPS was carried out using a Thermo Scientific K-Alpha spectrometer. Spectra were obtained using an aluminum anode ($\text{Al K}\alpha = 1486.6 \text{ eV}$) operated at 72 W and a spot size of 400 μm . The binding energies were referenced to C 1s of sp^3 carbon at 284.8 eV.

Electrochemical measurements. The electrochemical measurements were carried out on an Autolab PGSTAT 302 N electrochemical workstation connected to a three-electrode cell. A glassy carbon rotating disc electrode (4 mm diameter), a Ag/AgCl electrode filled with 3 M KCl solution, and a glassy carbon rod were used as the working electrode, the reference electrode, and the counter electrode, respectively. The working electrode was modified with a catalyst ink suspension to obtain a catalyst loading of 0.24 mg cm^{-2} . Typically, the catalyst ink suspensions were prepared by ultrasonically dispersing 3 mg sulfur-containing transition metal (hydr)oxide in 500 μL Nafion solution composed of 2 v% Nafion solution (5%, Aldrich), 49 v% H_2O , and 49 v% ethanol. Carbon nanotubes were added to the ink suspension (0.2 mg CNT/mL) to study their effects on the OER performance of sulfur-containing transition metal (hydr)oxides when needed. For comparison, a commercial ruthenium oxide (Aldrich) was also tested. All the electrochemical measurements were performed in a 1.0 M KOH solution ($\text{pH} = 13.6$) at room temperature with a rotating speed of 2500 rpm. Experiments were carried out in triplicates. Typically, 100 cyclic voltammetry (CV) scans (1.11 – 1.71 V versus RHE, 100 mV s^{-1}) were conducted to stabilize the catalyst, then a CV scan (1.11 – 1.86 V versus RHE, 5 mV s^{-1}) was applied to collect the polarization curve (positive potential sweep). Double layer capacitances (C_{dl}) were extracted from the CV scans in a non-faradaic potential range at various scan rates. Electrochemical impedance spectroscopy (EIS) was measured over a frequency range of 100 kHz to 50 mHz at 1.61 V versus RHE with an amplitude of the sinusoidal voltage perturbation of 10 mV. The catalytic stability was evaluated by chronoamperometry at 1.58 V versus RHE. The potentials were corrected with IR compensation to RHE by the formula $V_{\text{RHE}} (\text{V}) = V_{\text{Ag}/\text{AgCl}} + 0.21 \text{ V} + 0.059 \times \text{pH} - I \times R_s$.

Acknowledgments

Feng Zeng acknowledges the China Scholarship Council for financial support. Regina Palkovits, Cornelia Broicher, and Feng Zeng acknowledge the Federal Ministry of Education and Research (BMBF) for funding part of this work with the MANGAN research cluster BMBF-PTJ FKZ 03SF0508.

Conflict of Interest

The authors declare no conflict of interest.

Keywords: oxygen evolution reaction · OER · sulfur-containing · transition metal oxides · transition metal hydroxides

- [1] J. D. Holladay, J. Hu, D. L. King, Y. Wang, *Catal. Today* **2009**, 139, 244.
- [2] J. A. Turner, *Science* **2004**, 305, 972.
- [3] I. Roger, M. A. Shipman, M. D. Symes, *Nat. Rev. Chem.* **2017**, 1, 0003.
- [4] N.-T. Suen, S.-F. Hung, Q. Quan, N. Zhang, Y.-J. Xu, H. Ming Chen, *Chem. Soc. Rev.* **2017**, 46, 337.
- [5] S. Park, Y. Shao, J. Liu, Y. Wang, *Energy Environ. Sci.* **2012**, 5, 9331.
- [6] M. Tahir, L. Pan, F. Idrees, X. Zhang, L. Wang, J.-J. Zou, Z. L. Wang, *Nano Energy* **2017**, 37, 136.
- [7] M. H. Miles, E. A. Klaus, B. P. Gunn, J. R. Locker, W. E. Serafin, S. Srinivasan, *Electrochim. Acta* **1978**, 23, 521.
- [8] E. Antolini, *ACS Catal.* **2014**, 4, 1426.
- [9] N. Mamaca, E. Mayousse, S. Arrhi-Clacens, T. W. Napporn, K. Servat, N. Guillet, K. B. Kokoh, *Appl. Catal. B* **2012**, 111–112, 376.
- [10] C.-W. Tung, Y.-Y. Hsu, Y.-P. Shen, Y. Zheng, T.-S. Chan, H.-S. Sheu, Y.-C. Cheng, H. M. Chen, *Nat. Commun.* **2015**, 6, 8106.
- [11] F. Song, L. Bai, A. Moysiadou, S. Lee, C. Hu, L. Liardet, X. Hu, *J. Am. Chem. Soc.* **2018**, 140, 7748.
- [12] M. Gong, H. Dai, *Nano Res.* **2015**, 8, 23.
- [13] F. Lu, M. Zhou, Y. Zhou, X. Zeng, *Small* **2017**, 13, 1701931.
- [14] A. Sivanantham, P. Ganesan, S. Shanmugam, *Adv. Funct. Mater.* **2016**, 26, 4661.
- [15] X. Lv, Y. Zhu, H. Jiang, X. Yang, Y. Liu, Y. Su, J. Huang, Y. Yao, C. Li, *Dalton Trans.* **2015**, 44, 4148.
- [16] H. Liang, F. Meng, M. Cabán-Acevedo, L. Li, A. Forticaux, L. Xiu, Z. Wang, S. Jin, *Nano Lett.* **2015**, 15, 1421.
- [17] S. Chen, J. Duan, P. Bian, Y. Tang, R. Zheng, S.-Z. Qiao, *Adv. Energy Mater.* **2015**, 5, 1500936.
- [18] M. Zhou, Q. Weng, X. Zhang, X. Wang, Y. Xue, X. Zeng, Y. Bando, D. Golberg, *J. Mater. Chem. A* **2017**, 5, 4335.
- [19] C. Tang, H.-S. Wang, H.-F. Wang, Q. Zhang, G.-L. Tian, J.-Q. Nie, F. Wei, *J. Adv. Mater.* **2015**, 27, 4516.
- [20] K. Fan, Y. Ji, H. Zou, J. Zhang, B. Zhu, H. Chen, Q. Daniel, Y. Luo, J. Yu, L. Sun, *Angew. Chem.* **2017**, 56, 3289.
- [21] Y. Pi, Q. Shao, P. Wang, F. Lv, S. Guo, J. Guo, X. Huang, *Angew. Chem.* **2017**, 129, 4573.
- [22] L. Xu, Q. Jiang, Z. Xiao, X. Li, J. Huo, S. Wang, L. Dai, *Angew. Chem.* **2016**, 55, 5277.
- [23] X. Cui, P. Ren, D. Deng, J. Deng, X. Bao, *Energy Environ. Sci.* **2016**, 9, 123.
- [24] P. Cai, J. Huang, J. Chen, Z. Wen, *Angew. Chem.* **2017**, 56, 4858.
- [25] L. Fang, W. Li, Y. Guan, Y. Feng, H. Zhang, S. Wang, Y. Wang, *Adv. Funct. Mater.* **2017**, 27, 1701008.
- [26] W. Liu, Y. Hou, Z. Lin, S. Yang, C. Yu, C. Lei, X. Wu, D. He, Q. Jia, G. Zheng, X. Zhang, L. Lei, *ChemSusChem* **2018**, 11, 1479.
- [27] Y. Wang, C. Xie, Z. Zhang, D. Liu, R. Chen, S. Wang, *Adv. Funct. Mater.* **2017**, 28, 1703363.
- [28] Y. Hou, M. Qiu, T. Zhang, X. Zhuang, C.-S. Kim, C. Yuan, X. Feng, *Adv. Mater.* **2017**, 29, 1701589.
- [29] C. C. McCrory, S. Jung, J. C. Peters, T. F. Jaramillo, *J. Am. Chem. Soc.* **2013**, 135, 16977.
- [30] A. Bergmann, E. Martinez-Moreno, D. Teschner, P. Chernev, M. Gliech, J. F. de Araújo, T. Reier, H. Dau, P. Strasser, *Nat. Commun.* **2015**, 6, 8625.

- [31] B. J. Lindberg, K. Hamrin, G. Johansson, U. Gelius, A. Fahlman, C. Nordling, K. Siegbahn, *Phys. Scr.* **1970**, *1*, 286.
- [32] A. M. de Jong, H. J. Borg, L. J. van IJendoorn, V. G. F. M. Soudant, V. H. J. de Beer, J. A. R. van Veen, J. W. Niemantsverdriet, *J. Phys. Chem.* **1993**, *97*, 6477.
- [33] I. Alstrup, I. Chorkendorff, R. Candia, B. S. Clausen, H. Topsøe, *J. Catal.* **1982**, *77*, 397.
- [34] B. R. Strohmeier, D. M. Hercules, *J. Phys. Chem.* **1984**, *88*, 4922.
- [35] A. Matamoros-Veloza, O. Cespedes, B. R. G. Johnson, T. M. Stawski, U. Terranova, N. H. de Leeuw, L. G. Benning, *Nat. Commun.* **2018**, *9*, 3125.
- [36] R. B. Shalvoy, P. J. Reucroft, *J. Vac. Sci. Technol.* **1979**, *16*, 567.
- [37] S. Jin, *ACS Energy Lett.* **2017**, *2*, 1937.
- [38] F. Zeng, C. Broicher, S. Palkovits, K. Simeonov, R. Palkovits, *Catal. Sci. Technol.* **2018**, *8*, 367.
- [39] I. C. Man, H.-Y. Su, F. Calle-Vallejo, H. A. Hansen, J. I. Martínez, N. G. Inoglu, J. Kitchin, T. F. Jaramillo, J. K. Nørskov, J. Rossmeisl, *ChemCatChem* **2011**, *3*, 1159.
- [40] A. Vojvodic, J. K. Nørskov, *Science* **2011**, *334*, 1355.

Manuscript received: August 15, 2019
 Revised manuscript received: October 25, 2019
 Accepted manuscript online: October 25, 2019
 Version of record online: December 19, 2019
